

Statistical Global Model of β^- Halfives and r-Process Nucleosynthesis*

N. J. Costiris[†] and E. Mavrommatis[‡]
*Department of Physics, Section of Nuclear & Particle Physics
University of Athens, 15771 Athens, Greece*

K. A. Gernoth[§]
Institute for Theoretical Physics, Johannes Kepler University Linz, A-4040 Linz, Austria

J. W. Clark[¶]
*McDonnell Center for the Space Sciences and Department of Physics
Washington University, St. Louis, Missouri 63130, USA*

(Dated: June 24, 2013)

Background: Reliable prediction of outcomes of stellar nucleosynthesis via the rapid neutron-capture process (r-process) continues to present major challenges to nuclear astrophysics. Uncertainties still persist with respect to the astrophysical sites and the required nuclear-physics inputs. Principally, these inputs involve β -decay rates of neutron-rich nuclei, to which both the element distribution on an r-process path and the time scale of the r-process are highly sensitive. Since the majority of nuclides lying on an r-process path are not yet accessible experimentally, accurate forecasts of nuclear inputs based on well-tested global models are essential.

Purpose: Our objective is to apply an improved statistical global model of β^- -decay half-life systematics [1] generated by machine-learning techniques to the prediction of β half-lives relevant to r-process nuclei. The primary aim of this application is to complement existing r-process-clock and matter-flow studies, thereby providing additional theoretical support for the planning of future activities of the world’s network of rare-isotope laboratories.

Method: The statistical model employed in this investigation is rooted in a fully connected, multilayer artificial neural network having feed-forward perceptron architecture [3 – 5 – 5 – 5 – 5 – 1 [116]. The network model has been taught the systematics of β^- decay based on a subset of the existing data by implementing the optimal Levenberg-Marquardt learning algorithm together with Bayesian regularization and cross-validation. The target domain for the modeling is the half-life systematics of nuclear ground states that decay 100% by the β^- mode, with cutoff at 10^6 s.

Results: Results are presented for nuclides situated on the r-ladders at $N = 50, 82,$ and 126 where abundances peak, as well as for nuclides that affect abundances between peaks or may be relevant to r-processes under different astrophysical scenarios. The half-lives of some of the targeted neutron-rich nuclides have either been recently measured or will be accessible at rare-isotope laboratories in the relatively near future. The results of our large-scale data-driven half-life calculations (generated by a “theory-thin” global statistical model) are compared to available experimental data, including recent measurements on very neutron-rich nuclei along an r-process path far from the valley of β stability. Comparison is also made with corresponding results from traditional global models derived by semi-phenomenological “theory-thick” approaches.

Conclusions: Further evidence is presented that “theory-thin,” data-driven statistical global modeling of half-lives and other nuclear properties developed by machine-learning techniques can yield reliable predictions that may serve as inputs to different astrophysical scenarios for the r-process.

PACS numbers: 23.40.-s, 21.10.Tg, 26.30.Hj, 98.80.Ft, 07.05.Mh

Keywords: beta-decay half-lives, r-process nucleosynthesis, exotic nuclei, statistical modeling, neural networks

I. INTRODUCTION

Proposed more than fifty years ago, the r-process (short for “rapid neutron capture process”) is believed to be the origin of almost half the observed elemental abundances beyond iron [2–6]. The r-process abundance dis-

tributions (isotopic and isobaric) are normally deduced by subtracting the calculated s- and p-process contributions from the observed solar system abundances. Additionally, isotopic abundances characteristic of the early Galaxy are directly observed in metal-poor Eu-enriched halo stars (MPEES). A fairly robust main r-process operating over the history of the Galaxy is suggested by the consistency of the MPEES abundance patterns from star to star with the solar system r-process abundances for the heavier neutron-capture elements $A \geq 130$ (Ba and above).

In spite of the numerous studies of the r-process carried out to date, there still exist substantial uncertainties

* <http://www.pythaim.phys.uoa.gr>; pythaim@phys.uoa.gr

† ncost@phys.uoa.gr

‡ emavrom@phys.uoa.gr

§ klaus.a.gernoth@manchester.ac.uk

¶ jwc@wuphys.wustl.edu

about the underlying mechanism and the astrophysical sites where it takes place. Since the r-process is thought to occur in environments featuring a very high density of free neutrons, potential sites are associated with core-collapse supernovae. These include the neutrino-driven wind in delayed explosion models, relativistic jets arising in failed supernovae, and magnetohydrodynamic jets from supernovae. Alternatively, the r-process could also occur in mergers of two neutron stars, black-hole-neutron-star mergers, γ -ray bursts, or quark novae (for recent reviews, see Refs. [6, 7]). These diverse sites are inferred from corresponding models which, in addition to contrasting astrophysical conditions, differ in the nuclear-physics inputs employed in the calculations. According to the classical r-process model as first proposed, which is site invariant, the r-process path is dynamically determined by the temperature and the neutron densities. The equilibrium $(n, \gamma) \leftrightarrow (\gamma, n)$ fixes the path to very neutron-rich isotopes with one-neutron separation energies S_n of 2–3 MeV. The nuclei within an isotonic chain at which local abundance peaks are called waiting-point nuclei and correspond to closed neutron shells ($N=50, 82, 126$). At such points the r-process flow pauses for several hundred ms (whereas the average time between two neutron captures is ~ 1 ms), since the neutron capture cross-sections are extremely small. The r-process path climbs to higher Z nuclei as on a ladder, until it reaches an isotope at which it breaks out of the magic shell via subsequent neutron captures. At “freeze out,” where the temperature drops or the neutron density is quenched, the material decays back to stability via β -decay, producing the observed r-process abundances. The paths at $A \simeq 80, 130,$ and 195 originate mainly from the $N = 50, 82,$ and 126 progenitor isotopes around $^{80}\text{Zn}, ^{130}\text{Cd},$ and ^{195}Tm , respectively.

It is evident from these considerations that various input parameters from nuclear physics are indispensable for the calculation of the r-process abundances, depending on the astrophysical model adopted. During the equilibrium phase the most important quantities are masses (providing neutron separation energies and Q -values) and the half-lives $T_{1/2}$ of the participating nuclei. The masses determine the reaction path of the process, whereas the half-lives of the waiting-point nuclei determine how much material is transferred from one isotopic chain to another, and hence the progenitor abundances. In the “freeze out” phase, β -delayed neutron emission probabilities are needed since they divert the β -decay chains into neighboring nuclei and alter the observed abundance curve. Additionally, for nuclides above $A \geq 210$, neutron-capture cross-sections and alpha-decay half-lives are needed while for nuclides with $Z > 80$, fission parameters such as barriers, β -delayed fission probabilities, and neutron-induced fission cross-sections are involved. The end of the r-process, strongly model-dependent, is reached when the Coulomb energy becomes too large, most probably in the charge-mass region around $Z = 94, A = 270$. There, the r-process

material is recycled back into the $A \sim 130$ region by neutron-induced, beta-delayed, and spontaneous fission (“fission recycling”).

In this paper, we focus on the half-lives of nuclides involved in the r-process. As already indicated, knowledge of β^- half-lives T_{β^-} of heavy neutron-rich nuclides is essential to a thorough understanding of the r-process, due to their crucial role in determination of the time scale for matter flow and the abundances of heavier nuclei. Since very-neutron-rich nuclei far from the valley of stability participate in the r-process, the available experimental information on relevant T_{β^-} values has been quite limited, owing to the difficulty of the required measurements. Principally, data have been available in those regions where the reaction path approaches the stable valley, specifically at or near the shell closures at $N = 50, 82,$ and 126 . The pioneering experiments on isotopes along such a reaction path involved measurement, at ISOLDE, of the half-lives of the $N = 50$ isotopes ^{79}Cu and ^{80}Zn and the $N = 82$ isotopes ^{129}Ag and ^{130}Cd . All relevant experimental T_{β^-} half-lives available up to November 2003 are accessible in NUBASE2003 (hereafter denoted NUBASE03) [8].

Experimental data on β half-lives have subsequently been obtained mainly at NSCL at MSU, ISOLDE at CERN, GANIL, and RIKEN. We refer to those related to the r-process in Sect. III. Currently, experiments performed at existing radioactive-ion facilities (Rex-ISOLDE at CERN, FRS/ESR at GSI, RIBF at RIKEN) are under analysis, and further β^- half-life measurements are scheduled. More advanced radioactive-beam facilities will come into operation in the relatively near future, with increased yields by factors up to 1000 (FAIR at GSI, FRIB at MSU and RIBF at RIKEN [9]). In spite of the increasing experimental activity, many neutron-rich nuclides contributing to the r-process will remain inaccessible to measurement for some time to come. Accordingly, continued progress in modeling the r-process rests on reliable predictions from macroscopic/microscopic models of nuclear systematics based on fundamental nuclear theory and estimates provided by innovative methods of statistical inference adapted to the problem domains of β -decay half-lives and other relevant nuclear observables.

A number of useful approaches to traditional calculation of β -decay half-lives within state-of-the-art nuclear theory have been proposed and applied in different regions of the nuclear chart. These include the more phenomenological treatments, such as the gross theory (GT), as well as microscopic approaches based on the shell model and the proton-neutron quasi-particle random-phase approximation (pn QRPA) in various versions. Some of these approaches emphasize only global applicability, while others seek self-consistency or comprehensive inclusion of nuclear correlations. In the following we call attention to the most recent theoretical calculations within these categories and invoke their results as standards for comparison throughout the pa-

per. Additionally, a brief review of a number of conventional theoretical models of β -decay systematics may be found in Ref. [1]. In the shell model (SM) calculations of Ref. [10], the detailed structure of the beta strength function is considered and results are given for nuclei at neutron number $N = 82$. The size of the configuration space sets limits such that calculations for heavy nuclei are become impractical. In the hybrid model of Möller and co-workers [11], the study of the nuclear ground state is based on the finite-range droplet model (FRDM) and a folded-Yakawa single-particle potential. The β -decay half-lives for the allowed Gamow-Teller transitions are obtained from a pn QRPA calculation after the addition of pairing and Gamow-Teller residual interactions, whereas the effect of the first-forbidden (ff) transitions is included by means of the statistical gross theory (pn QRPA+ ff GT). Results are derived for nuclides in the range $8 < Z \leq 110$ and $11 \leq N \leq 229$. Borzov and co-workers have developed procedures for determining ground-state properties and Gamow-Teller and ff transitions of nuclei based on a density functional plus continuum QRPA (DF3+CQRPA) approximation, with the spin-isospin effective NN interaction of finite Fermi system theory operating in the ph channel. This approach has been applied near closed neutron shells at $N = 50, 82, 126$, and in the region “east” of ^{208}Pb [12, 13]. These approaches are non relativistic. In the relativistic framework, there is a recent pn QRPA calculation (pn RQRPA) of the Gamow-Teller β -decay half-lives based on a relativistic Hartree-Bogoliubov description of nuclear ground states that involves a density-dependent effective interaction DD-ME1* and includes momentum-dependent nuclear self-energies. This treatment has been applied in the calculation of β -decay half-lives T_{β^-} of neutron-rich even-even nuclei in the $Z \sim 28$ and $Z \sim 50$ regions [14].

Although conventional theory shows continuing improvement, especially with respect to the evaluation of ff transitions, the predictive power of these “theory-thick” models is rather limited far from stability. Most cases permitting calculation exhibit sensitivity to input quantities that are poorly known. Given this situation, “theory-thin” data-driven statistical modeling based on artificial neural networks (ANNs), and other machine-learning techniques of statistical inference such as support-vector machines, offers a potentially effective alternative for global modeling of β^- -decay lifetimes. Such approaches have proven effective in statistical modeling of other nuclear properties (including atomic masses, neutron separation energies, ground-state spin and parity, and branching probabilities for different decay channels), as well as in a variety of other scientific problem domains [15, 16]. The β -decay half-life is in principle determined as a mapping from the atomic and neutron numbers Z and N identifying a nuclide to its corresponding value T_{β^-} , and one constructs an approximation to this mapping based on a *subset* of the available data (called the training or learning set). Statistical global models of this kind have previously been applied to the β -decay problem in

Refs. [1, 17, 18].

The findings of this paper are based on our most recent ANN statistical global model of T_{β^-} systematics for the half-lives of nuclear ground states that decay 100% by the β^- mode (referred to as the standard ANN model) [1]. This model has been developed by implementing a number of advances in machine-learning algorithms. Here it will be applied in a comprehensive study of the β^- half-lives of nuclides relevant to the r-process. The results are compared with the available experimental data and with corresponding predictions from “theory-thick” models as cited above. The ANN model exhibits good behavior in terms of several important performance measures. In a purely results-oriented sense, its predictive accuracy matches or surpasses that of traditional models based on microscopic nuclear theory and phenomenology. Accordingly, the ANN model serves to complement and support the traditional “theory-thick” models, which have the further aim of providing valuable insight into the underlying physics. Section II describes the essential features of our model. Results for the half-lives of r-process nuclides are reported and discussed in Sect. III. Finally, Sect. IV summarizes the conclusions of the present study.

II. THE MODEL

A. General

Inspired by natural neural systems, an artificial neural network (ANN) consists of interconnected dynamical units (usually called neurons) that are typically arranged in a distinct layered topology and characterized by soft-threshold nonlinear response to weighted and summed inputs. The pattern of weighted connections between the units (along with unit biases) determines the function of the network. The network employed in the present work is a multilayer *feed-forward* ANN [19], thus a multilayer perceptron, whose gross architecture can be summarized by the notation

$$[I - H_1 - H_2 - \dots - H_L - O | W], \quad (2.1)$$

where I is the number of inputs, H_i is the number of neurons in the i^{th} hidden layer, O is the number of outputs, and W is the total number of parameters needed to complete the specification of the network in terms of the weights w_{ij} of the connections and the biases b_i of the units. In global nuclear modeling, ANNs can perform two kinds of tasks: classification and function approximation (or regression), the former being a special case of the latter. In the latter, any nuclear observable can be viewed as a mapping from a set of independent variables identifying an arbitrary nuclide (here, proton and neutron numbers Z and N), to the corresponding dependent variable chosen for study (here, the β^- half-life of the ground state of the parent nucleus). The function so defined is determined by the set of parameters $\{w_{ij}, b_i\}$,

whose values are derived during the learning (or training) phase by applying a suitable machine-learning algorithm to minimize some appropriate measure (called a cost function or objective function) of the errors made by the network in response to inputs corresponding to a set of examples or “training patterns” chosen from the mapping $(Z, N) \rightarrow T_{\beta^-}$. A network created by such a supervised learning scheme is said to exhibit good generalization or prediction if it performs well for inputs (nuclides) belonging to a test set disjoint from the training set. Statistical modeling of this sort inevitably involves a trade-off between closely fitting the training data and performing reliably in interpolation and extrapolation, i.e., in generalization. To enhance generalization, we employ a third set of patterns, called the validation set, which includes nuclides disjoint from both the training and test sets.

B. ANN for T_{β^-} values

In Ref. [1] we have developed a fully connected feed-forward artificial neural network with architecture symbolized by $[3 - 5 - 5 - 5 - 5 - 1 | 116]$ that generates T_{β^-} values for given nuclides. The activation functions of the processing units (model neurons) of the network are taken to be of hyperbolic-tangent-sigmoid form in the four intermediate hidden layers, a saturated linear function being chosen for the single neuron of the output layer. Using existing β^- data, this network has been taught with the Levenberg-Marquardt back-propagation learning algorithm [20], a procedure which has the fastest convergence in function-approximation problems. Our goal in training was not simply to attain an exact reproduction of the known half-lives, but rather to achieve an accurate representation of the regularities inherent in the target mapping, thereby promoting generalization. To this end, we have employed two well established techniques for avoiding over-fitting, namely cross-validation and Bayesian regularization. The method of Nguyen and Widrow [21] has been used to initialize the free network parameters (its weights and biases) whereas the batch mode has been adopted for their iterative updating. The input coding scheme represents Z and N as analog variables, scaled to fit within the sensitive range $[-1, 1]$ of the activation function assigned to two of the three input units. Retaining the spirit of stand-alone, “theory-thin” modeling driven purely by the data, a third input unit is added to represent the delta-parameter, which is defined as the mean of the parities of Z and N . Implementation of this parity unit facilitates the recognition of pairing and shell effects. The base-10 logarithm of the β^- half-life calculated by the network is represented by the activity of the single analog output unit. The inference process performed by the ANN model can therefore be epitomized in the expression:

$$\log_{10} T_{\beta}(Z, N) = \tilde{g}(Z, N, \delta) + \tilde{\varepsilon}(Z, N, \delta), \quad (2.2)$$

where $\tilde{g}(Z, N, \delta)$ is the function that decodes the decay information and $\tilde{\varepsilon}(Z, N, \delta)$ is a random expectation error that represents our ignorance about the dependence of T_{β^-} on Z and N . This ε “noise” term may reflect numerous small-scale influences on the phenomenon that are “effectively chaotic,” along with regularities missed in the training process.

C. Data Sets

The performance of such a statistical modeling approach necessarily depends on both the quantity and quality of the training data. The experimental β^- -decay half-life values used in our ANN modeling have been taken from the NUBASE03 compilation of nuclear and decay properties [8] carried out by Audi and co-workers at the Atomic Mass Data Center. Attention is restricted to the ground states of parent nuclei that decay 100% by the β^- mode (NuSet-A). We have considered several subsets of this specific database. The best data set that we have finally adopted in constructing and testing our standard ANN model [1] is NuSet-B, consisting of 838 nuclides ranging from ^{35}Na to ^{247}Pu and derived from NuSet-A by applying a cut-off at 10^6 s. Without significant detriment to the prediction of β^- half-lives, this creates a more homogeneous collection of nuclides and thereby facilitates training of the network. NuSet-B is further subdivided randomly into three subsets with 503 nuclides ($\sim 60\%$) used for training the network (training or learning set) and 167 nuclides ($\sim 20\%$) used to assess the training procedure (validation set), the remaining 168 nuclides ($\sim 20\%$) being reserved to evaluate the accuracy of prediction (test set).

D. Performance

The performance of our global ANN model is first evaluated by direct comparison with experimental data in terms of commonly used measures of statistical analysis, namely the root-mean-square error (σ_{rms}), the mean absolute error (σ_{ma}), and the normalized mean-square error (σ_{nms}), as well as the correlation coefficient R for

TABLE I. Performance measures for the learning, validation, test, and whole sets, achieved by the standard ANN model of Ref. [1], a network with architecture $[3 - 5 - 5 - 5 - 5 - 1 | 116]$ trained on nuclides from NuSet-B.

Performance Measure	Learning Set	Validation Set	Test Set	Whole Set
σ_{rms}	0.53	0.60	0.65	0.57
σ_{nms}	1.004	0.995	1.012	0.999
σ_{ma}	0.38	0.41	0.46	0.40
R	0.964	0.953	0.947	0.958

a linear regression analysis. Table I collects results for these overall quality measures for the learning, validation, test sets, as well as the whole set (NuSet-B). More problem-specific quality measures that have been introduced in the literature for global modeling of β^- half-lives have also been evaluated within prescribed half-life domains. Specifically, these are the quantities x_K and σ_K , $M^{(10)}$, $\sigma_M^{(10)}$, and $\Sigma^{(10)}$ defined and employed by Klapdor and co-workers [22] and Möller and co-workers [11] respectively, and re-examined quantitatively for both traditional and ANN models in Ref. [1]. Analysis of the performance of the standard network model for NuSet-B confirms a balanced behavior of network response in all β^- -decay regions, with relatively small discrepancies between calculated and observed β^- half-lives. Comparison of this behavior with that of “theory-thick” global models demonstrates that in a clear majority of cases, our standard statistical ANN model of β^- half-life systematics makes predictions that are closer to experiment. This may be partially ascribed to its larger number of adjustable parameters, although it should be emphasized that in general having more parameters leads to better fitting but not better prediction. Improved performance is also shown by the standard ANN model [1] relative to previous ANN models [17, 18]. This improvement is ascribed to its strategic advantages: different architecture and input encoding as well as a more advanced training procedure.

Clearly, the challenging goal of global modeling of nuclear properties, statistical or conventionally theoretical, is not only to reproduce the experimentally known β^- half-lives with some accuracy across the known nuclear landscape, but also to demonstrate good extrapolability (the ability to extrapolate away from existing data). Accordingly, further tests focusing on the performance of the ANN model in generalization have been carried out. These include assessment of performance on a set of “outlying” nuclides, not contained in NuSet-B, whose half-lives have been recently measured, as well as performance for nuclides along particular isotopic and isotonic chains. Also within this spirit, we have carried out two additional modeling studies for two other ANN models having the same architecture as the standard model, i.e., [3 – 5 – 5 – 5 – 5 – 1][116] [1]. All such tests indicate that the standard ANN model extrapolates satisfactorily, at least for nearby nuclei in the nuclear landscape. A detailed analysis of the quality of performance of this model has been provided in Ref. [1].

III. RESULTS & DISCUSSION

In this section we present our results for β^- half-lives T_{β^-} of nuclides relevant to the r-process, as generated by the ANN model. We compare these results with available experimental values as well as with half-lives given by the theoretical models highlighted in the introduction, namely those denoted $pnQRPA+ffGT$ [11],

$pnQRPA+ffGT$ [14], SM [10], and DF3+CQRPA [12]. First, we examine the results obtained for regions close to the waiting-points $N=50$, 82, and 126. A critical assessment of the predictive quality of the ANN model is made by examining its results for isotopic chains of several nuclides situated in these regions, as well as for some neighboring nuclides whose T_{β^-} have been measured *after* publication of the NUBASE03 database [8] used in the model’s construction. Looking to the future, T_{β^-} values are predicted (i) for nuclides that are being studied experimentally at FSR/ESR at GSI according to the proposals S323 [23] and S410 [24], and also (ii) for neutron-rich nuclides relevant to the r-process that have recently been identified at RIKEN [25] and at GSI [26], but whose T_{β^-} are yet to be measured.

A. Nuclei in the region of the $N=50$ closed neutron shell (around the $A \simeq 80$ peak)

Chart of nuclides up to $N = 50$

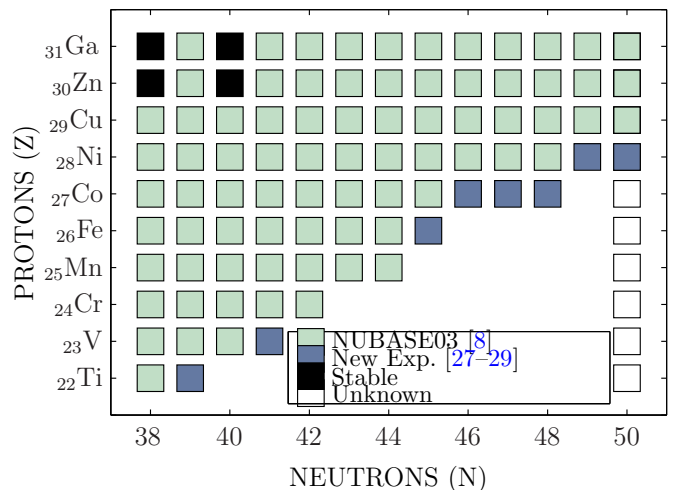


FIG. 1. (Color online) Cluster plot of the chart of nuclides up to the $N = 50$ closed shell. Black boxes indicate stable nuclides. Gray (green) boxes indicate the nuclides with measured β^- -decay half-lives T_{β^-} reported in NUBASE03 [8], while dark gray (blue) boxes identify those with newly measured T_{β^-} beyond NUBASE03 [27–29]. Empty boxes denote nuclides at the $N = 50$ closed shell for which no experimental β^- half-lives are available. Theoretical values for T_{β^-} from the standard ANN model, as well as from conventional nuclear models, are plotted in Fig. 2.

Neutron-rich nuclides in the region of the $N = 50$ closed neutron shell play an important role in r-process nucleosynthesis. In the classical r-process model, the $N = 50$ nuclides act as waiting-points and determine the formation and shape of the $A \simeq 80$ abundance peak with progenitor nuclide ^{80}Zn . In the newer site-dependent r-process models, involving a neutrino-driven wind and a high-entropy wind and extensions thereof, the r-process

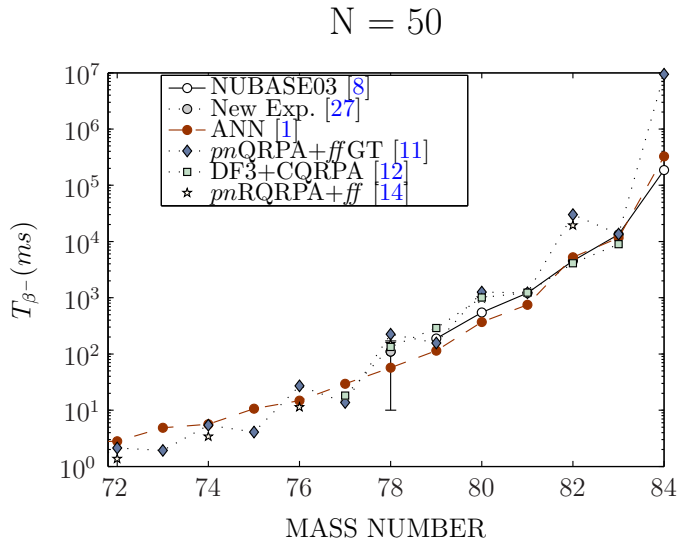


FIG. 2. (Color online) Beta-decay half-lives T_{β^-} produced by the ANN model for the r-ladder isotonic chain at $N = 50$ (from $Z = 22$ up to $Z = 34$) in comparison with experimental values [8, 27], and with corresponding results from $pnQRPA+ffGT$ [11], DF3+CQRPA [12] and $pnRQRPA+ff$ [14] calculations.

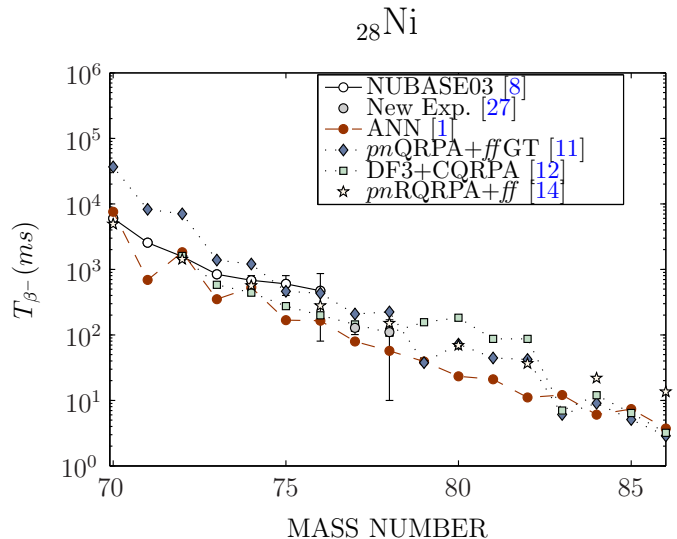


FIG. 4. (Color online) Beta-decay half-lives T_{β^-} produced by the ANN model for the isotopic chain of ${}_{28}\text{Ni}$ (from $N = 42$ up to $N = 58$) in comparison with experimental values [8, 27], and with corresponding results from $pnQRPA+ffGT$ [11], DF3+CQRPA [12] and $pnRQRPA+ff$ [14] (the last only for even-even nuclei) calculations.

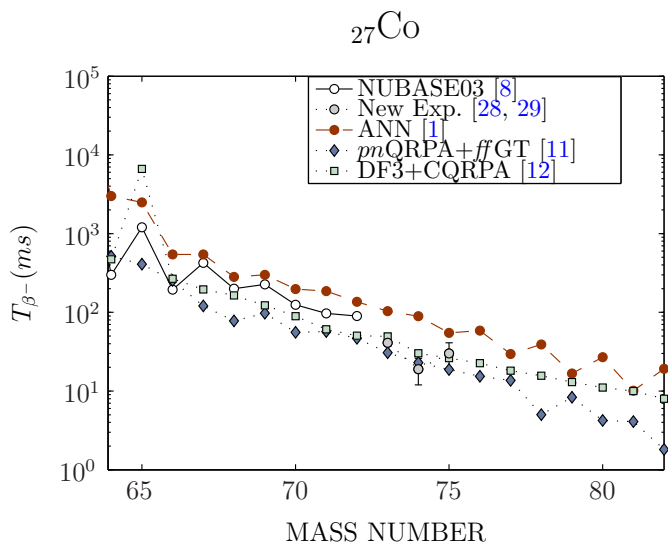


FIG. 3. (Color online) Beta-decay half-lives T_{β^-} produced by the ANN model for the isotopic chain of ${}_{27}\text{Co}$ (from $N = 37$ up to $N = 55$) in comparison with experimental values [8, 28, 29] and results from $pnQRPA+ffGT$ [11] and DF3+CQRPA [12] calculations.

begins at lighter nuclei, but the half-lives of waiting-point nuclides are a direct input and set the r-process time scale through the $N = 50$ bottleneck towards heavier nuclei.

A chart of nuclides up to the $N = 50$ closed shell with known experimental T_{β^-} is presented in Fig 1. Nuclides whose T_{β^-} value is included in NUBASE03 [8] are shown with gray (green) boxes. Nuclides with T_{β^-} values (not included in NUBASE03) but recently measured at

NSCL [27, 28] (${}^{75}\text{Co}$, ${}^{77,78}\text{Ni}$, ${}^{80}\text{Cu}$) and at GANIL [29] (${}^{61}\text{Ti}$, ${}^{64}\text{V}$, ${}^{71}\text{Fe}$, ${}^{73,74}\text{Co}$) are labeled in dark gray (blue). The half-lives for ${}^{73,74}\text{Co}$ have also been measured at NSCL [27], but we adopt here the most recently measured GANIL values.

These “beyond NUBASE03” values along with the corresponding predictions from our ANN model and those available from $pnQRPA+ffGT$ [11] and DF3+CQRPA[12] calculations are displayed in Table II. In these cases, the ANN is making true predictions rather than regurgitating approximate fits, since none of the nuclei involved were present in the training set or validation set.

One of the pivotal measurements in this isotopic region is the accurate determination of T_{β^-} for the doubly magic waiting-point nucleus ${}^{78}\text{Ni}$, carried out by an NSCL team at Michigan State University (MSU) [27]. This quantity is among those needed to disentangle the various contributions from neutron-capture processes in different astrophysical sites. It is of special importance since the time-scale for building heavy elements beyond $N = 50$ is set by the sum of the lifetimes of ${}^{78}\text{Ni}$ and ${}^{79}\text{Cu}$, and the shorter half-life found implies an acceleration of the r-process. It is seen from Fig. 1 that all important $N = 50$ waiting-pointing nuclei (${}^{78}\text{Ni}$, ${}^{79}\text{Cu}$, ${}^{80}\text{Zn}$) already have known experimental values for T_{β^-} , whereas this is not the case for the lighter nuclides. Fig. 2 shows the predictions from the ANN model for the isotonic chain at $N = 50$ (from $Z = 22$ up to $Z = 34$) and compares them with the available experimental values and with results from the three theoretical models $pnQRPA+ffGT$ [11], DF3+CQRPA [12], and (for even-even nuclei only) pn -

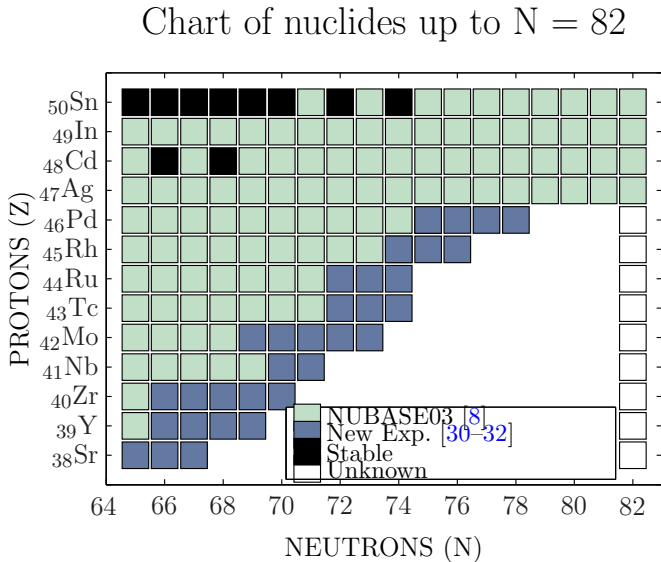


FIG. 5. (Color online) Cluster plot of the chart of nuclides up to the $N = 82$ closed shell. Black boxes indicate stable nuclides. Gray (green) boxes indicate the nuclides with measured β^- -decay half-lives T_{β^-} reported in NUBASE03 [8], while dark gray (blue) boxes indicate those with newly measured T_{β^-} beyond NUBASE03 [30–32]. Empty boxes denote nuclides at the $N = 82$ closed shell for which no experimental T_{β^-} values are available. Predicted values for the latter from our ANN model as well as calculated results from three theory-thick models are given in Fig. 6.

RQRPA+ ff [14]. Results provided by the ANN model are close to the experimental values and to the results of pn QRPA+ ff GT [11] and DF3+CQRPA [12] calculations. The T_{β^-} values obtained by Möller et al. [11] are larger than those given by the ANN model for $Z \geq 28$ and smaller for $Z < 28$, and they show more pronounced pairing behavior. The performance of our model in this region can also be evaluated by studying the isotopic chains of Co and Ni (see Figs. 3 and 4). The ANN model gives half-lives quite close to the experimental values and in most cases shows good agreement with results of the DF3+CQRPA [12] calculations.

B. Nuclei in the region of the $N = 82$ closed neutron shell (around the $A \simeq 130$ peak)

Reproduction of the abundances at the second peak (around $A \simeq 130$) is a major goal of theoretical research on r-process nucleosynthesis directly related to studies of β -decay of nuclei in the region of the $N = 82$ closed neutron shell. Each $N = 82$ r-process isotope acts as a waiting-point for different ranges of neutron density. Such studies have reached the r-process elements (Ag, Cd) and right wing (In, Sn, Sb, Te, I) at the top of the $A \simeq 130$ r-process peak. Recently β^- half-lives of very neutron-rich nuclides in the left wing have been determined experimentally, but measurements have not yet

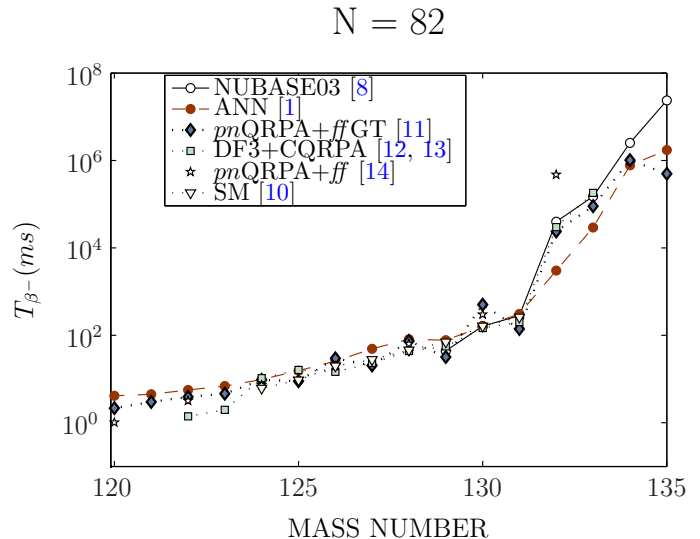


FIG. 6. (Color online) Beta-decay half-lives T_{β^-} produced by the standard ANN model for the r-ladder isotonic chain at $N = 82$ (from $Z = 38$ up to $Z = 53$) in comparison with experimental values [8], and with corresponding results from pn QRPA+ ff GT [11], DF3+CQRPA [12, 13], pn QRPA+ ff [14] (only for even-even nuclei), and SM [10] calculations.

reached the r-process path in this region. The left-wing region of nuclei, with $A \simeq 110 - 125$ up to the onset of the $A \simeq 130$ peak, is an especially interesting one for r-process physics, in the sense that within this range most astrophysical r-process models overestimate solar system isotopic abundances by an order of magnitude or more. This unrealistic trough has been attributed to a possible quenching of the $N = 82$ shell gap far from stability and to possible neutrino spallation effects [33]. In addition, there are indications from the abundance pattern in r-process-enhanced extremely metal-poor stars [34, 35] that a second r-process is needed to explain the solar abundance pattern in the $A = 90 - 130$ mass region. Moreover, galactic chemical models of the slow neutron capture process in stars on the asymptotic giant branch imply that at least one additional primary s-process is required in this mass region [36]. Good nuclear inputs, including β^- half-lives, are therefore required in order to distinguish the different neutron-capture processes and extract reliable information on them.

In recent years several experimental programs have focused on the region of the r-process path near $N = 82$. Beta-decay properties including β^- half-lives of exotic neutron-rich Kr, Sr, Y, Zr, Nb, Mo, and Tc nuclides have been studied at the RIBF facility at RIKEN [30]. Additionally, the half-lives of neutron-rich Ru, Rh, and Pd nuclides have been measured at NSCL [31]. It also should be mentioned that half-lives for $N \simeq 66$ mid-shell nuclei below $A \simeq 110$, i.e., for ^{105}Y , $^{106,107}\text{Zr}$, and ^{115}Tc , have been measured at NSCL [32] after publication of NUBASE03, but we consider here the most recent RIKEN measurements. In the chart of Fig. 5 the nuclides

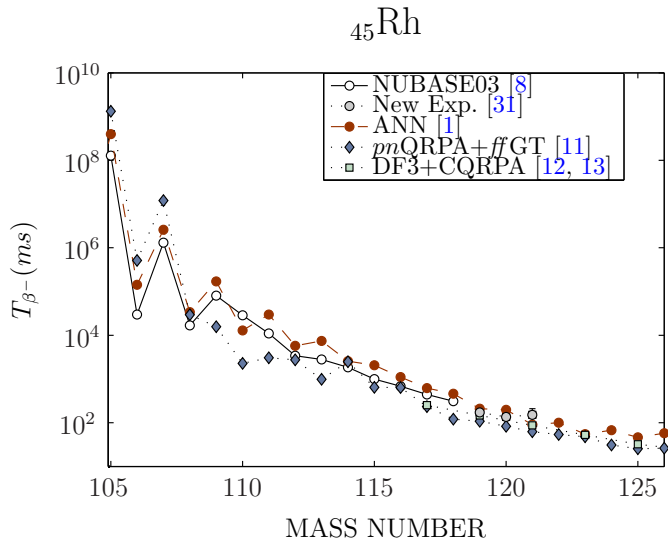


FIG. 7. (Color online) Beta-decay half-lives T_{β^-} produced by the ANN model for the isotopic chain of ^{45}Rh (from $N = 60$ up to $N = 81$) in comparison with experimental values [8, 31], and with corresponding results from $pn\text{QRPA}+ff\text{GT}$ [11] and $\text{DF3}+\text{CQRPA}$ [12, 13] calculations.

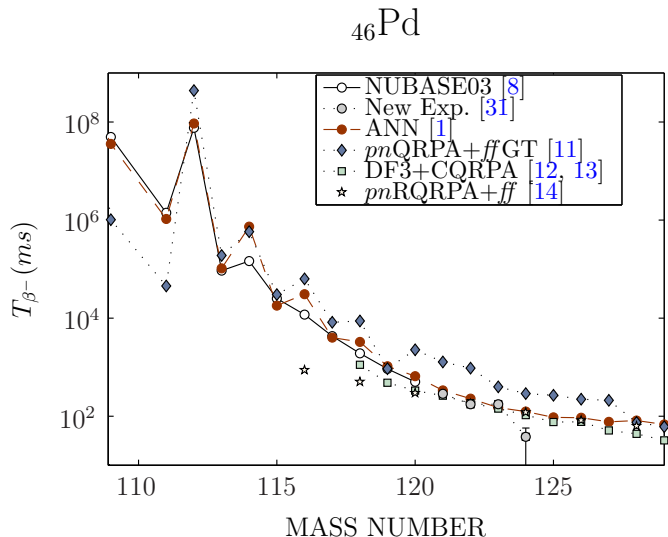


FIG. 8. (Color online) Beta-decay half-lives T_{β^-} produced by the ANN model for the isotopic chain of ^{46}Pd (from $N = 63$ up to $N = 83$) in comparison with experimental values [8, 31], and with results from $pn\text{QRPA}+ff\text{GT}$ [11], $\text{DF3}+\text{CQRPA}$ [12, 13], and (only for even-even nuclei) $pn\text{RQRPA}+ff$ [14] calculations.

named above are denoted by dark gray (blue) boxes, while other nuclides in this region whose T_{β^-} values have been measured earlier (and appear in NUBASE03 [8]) are symbolized by gray (green) boxes. In Table II we also list T_{β^-} values of r-process nuclides on the right wing of the $A \simeq 130$ peak not included in NUBASE03 but measured at CERN/ISOLDE. More specifically, the isotopes ^{133}Cd [42], ^{138}Sn [38], and $^{138-139}\text{Sb}$ [37] have been

studied. Very neutron-rich Cd, Sn, and Sb nuclides play a critical role in r-process nucleosynthesis calculations, as they lie directly on the path of the r-process under a wide range of astrophysical conditions. Table II provides a detailed comparison of the outputs of the standard ANN model and theoretical results (as available) from the $pn\text{QRPA}+ff\text{GT}$ [11] and $\text{DF3}+\text{CQRPA}$ [12, 13] calculations with the experimental β^- half-lives for all the recently measured nuclides identified in this paragraph. It is seen that most of the ANN predictions are closer to the measured values than those of the $pn\text{QRPA}+ff\text{GT}$ [11] model. This theory-thick model significantly overestimates the T_{β^-} values for the relevant Zr, Nb, and Mo isotopes, as is also the case for the relevant isotopes of Ru, Pd, Cd, Sn, and Sb. On the other hand, the ANN statistical model underestimates the β^- half-lives in almost all cases except Pd, but to a lesser extent.

We have considered above the half-lives of neutron-rich nuclides around the $N = 82$ r-process path that have recently been measured and therefore played no role in construction of the ANN model. The T_{β^-} values of the $N = 82$ isotones in the region $Z = 38 - 53$ that are experimentally known are displayed in Fig. 6. In the same figure the values generated by the ANN model for isotopes in the region $Z = 38 - 53$ are compared with the corresponding experimental results as well as with results from the $pn\text{QRPA}+ff\text{GT}$ [11], $\text{DF3}+\text{CQRPA}$ [12, 13], $pn\text{RQRPA}+ff$ [14] (only for even-even nuclei), and SM [10] calculations. For $Z < 50$ the T_{β^-} values from the various theory-thick calculations do not differ much. It is instructive to further evaluate the performance of the ANN model in this regime by considering the half-lives of nuclides in the isotopic chain of Rh and Pd (Figs. 7, 8). The T_{β^-} values produced by the ANN model are generally in better agreement with the available experimental measurements than those of Ref. [11] and are rather closer to the corresponding $\text{DF3}+\text{CQRPA}$ results [12, 13].

C. Nuclei in the region of the $N = 126$ closed neutron shell (around the $A \simeq 195$ peak)

The half-lives of heavy neutron-rich nuclides in the $N = 126$ region considerably below the doubly magic nucleus ^{208}Pb are also important for an understanding of the r-process. They play a key role in determining the relative $A = 195$ r-process peak abundances. They also determine how rapidly the heaviest nuclei are synthesized during the r-process (and hence the strength of “fission cycling” [39]), as well as the r-process end point.

Recently, experimental results in the $N = 126$ region obtained by cold fragmentation and a novel method of analysis [26, 39] have been reported by the RISING Collaboration (projects S227, S312) at GSI. There is the prospect of experimental measurements for more neutron-rich nuclides in this region with the advent of a new generation of in-flight secondary beam facilities, i.e., FAIR at GSI, RIBF at RIKEN, and FRIB at MSU [9].

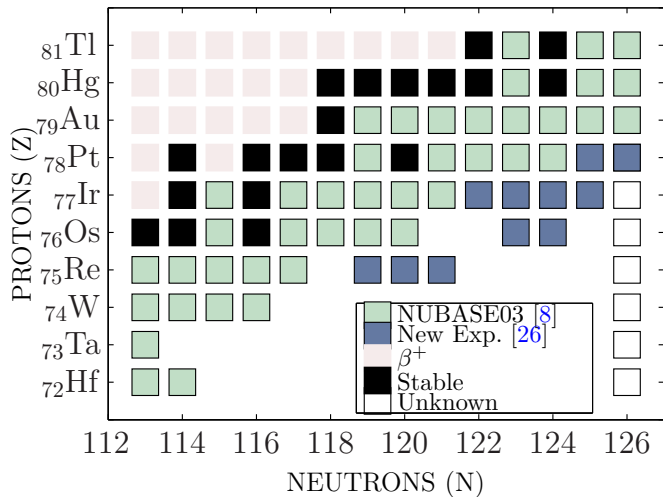
Chart of nuclides up to $N = 126$ 

FIG. 9. (Color online) Cluster plot of the chart of nuclides up to the $N = 126$ closed shell. Black boxes indicate stable nuclides. Gray (green) boxes indicate nuclides with measured β^- -decay half-lives T_{β^-} reported in NUBASE03 [8], while dark gray boxes (blue) identify those with newly measured T_{β^-} beyond NUBASE03 [26]. Empty boxes denote nuclides at the $N = 126$ closed shell for which no experimental T_{β^-} value is available. Theoretical values for T_{β^-} from the standard ANN model as well as from conventional nuclear models are plotted in Fig. 10.

A chart of nuclides up to the $N = 126$ closed shell with known experimental β^- -decay half-lives is displayed in Fig. 9. Nuclides whose T_{β^-} values are included in NUBASE03 [8] are represented by green [26, 39, 40] after publication of NUBASE03 are indicated in dark gray (blue). Specifically, these latter experimental half-lives include measurements for $^{194-196}\text{Re}$, $^{199-200}\text{Os}$, $^{199-202}\text{Ir}$, and $^{203-204}\text{Pt}$ and provide evidence for tests of ANN and traditional models of beta-decay systematics. Table II juxtaposes the predictions from the standard ANN model and from $pnQRPA+ffGT$ [11] and DF3+CQRPA [12] calculations, with the recent half-life data from GSI. In particular, the DF3+CQRPA calculation follows that for $N \simeq 126$ described in Ref. [12], being based on the Fayans energy-density functional but with no energy-dependent smearing in the treatment of Gamow-Teller and first-forbidden transitions. Fig. 10 compares the ANN predictions for the isotonic chain at $N = 126$ (from $Z = 72$ up to 81) with available experimental values and with results from the $pnQRPA+ffGT$ [11] and DF3+CQRPA calculations [12]. The ANN results are seen to be in better agreement with the experimental data than those of Möller et al. [11] (which for most of the nuclei are more than an order of magnitude larger than the data), and they show less pronounced odd-even staggering. Generally, the ANN model predicts shorter half-lives for $N = 126$ isotones than the $pnQRPA+ffGT$ model, thus implying that the

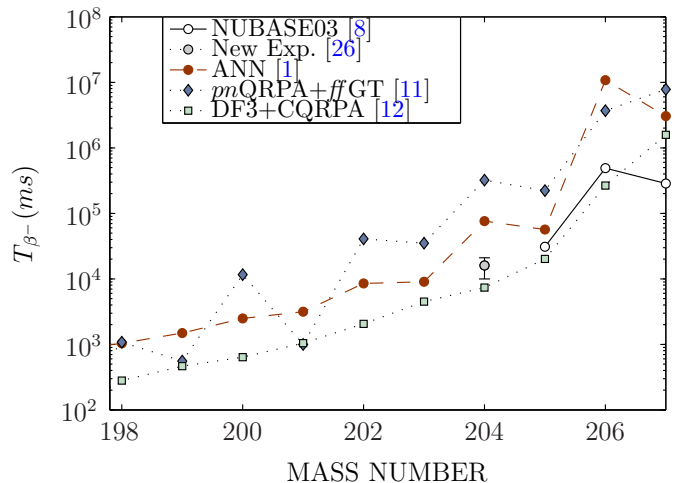
 $N = 126$ 

FIG. 10. (Color online) Beta-decay half-lives T_{β^-} produced by the ANN model for the r-ladder isotonic chain at $N = 126$ (from $Z = 72$ up to $Z = 81$) in comparison with experimental values [8, 26], and with results from $pnQRPA+ffGT$ [11] and DF3+CQRPA [12] calculations.

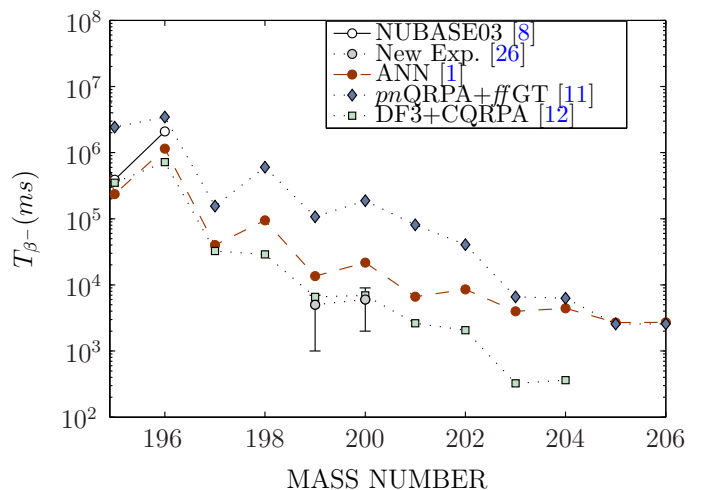
 ^{76}Os 

FIG. 11. (Color online) Beta-decay half-lives T_{β^-} produced by the ANN model for the isotopic chain of ^{76}Os (from $N = 119$ up to $N = 130$) in comparison with experimental values [8, 26], and with results from $pnQRPA+ffGT$ [11] and DF3+CQRPA [12] calculations.

matter flow to the heavier fissioning nuclides is faster. Compared to the results from the DF3+CQRPA calculations [12], the ANN values are generally somewhat larger. The performance of our model in this region can be further evaluated by studying the isotopic chains of Os and Ir (see Figs. 11 and 12, respectively). Generally, half-lives predicted by the ANN model are quite close to the experimental values, longer than those of the DF3+CQRPA calculations [12] but shorter than those of

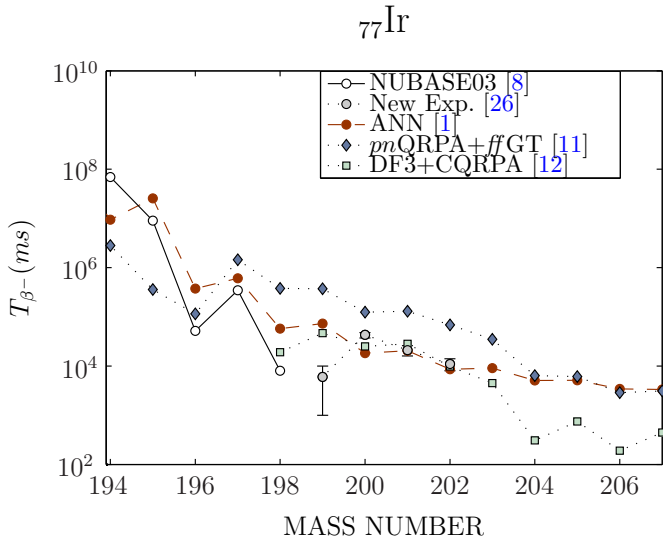


FIG. 12. (Color online) Beta-decay half-lives T_{β^-} given by the ANN model for the isotopic chain of ^{77}Ir (from $N = 117$ up to $N = 130$) in comparison with experimental values [8, 26], and with results from $pnQRPA+ffGT$ [11] and $DF3+CQRPA$ [12] calculations.

the $pnQRPA+ffGT$ [11] model, the latter behavior being exhibited especially for Os isotopes with $A \leq 202$ and for Ir isotopes with $197 \leq A \leq 203$. (One could say that the ANN interpolates between the two theory-thick models.) The good agreement of the results of the ANN model with the experimental half-lives in this region of the nuclear chart, as well as with those in the $N = 50$ and $N = 82$ regions, gives some confidence in the values extracted for the $N = 126$ r-process waiting-points.

In the previous sections the ANN model has been employed (i) to generate statistically derived values of the half-lives of neutron-rich nuclei close to the waiting-point nuclei at $N = 50, 82$, and 126 that have recently been measured, and (i) to predict the half-lives of the rest of the waiting-point nuclei at $N = 50, 82$, and 126 . Experimental values of T_{β^-} for nuclei not included in NUBASE03, along with the predicted half-life values produced by the ANN model and calculated values from two conventional nuclear models ($pnQRPA+ffGT$ [11] and $DF3+CQRPA$ [12]) are also listed in Table II. Based on the reported values of the error measure σ_{rms} (0.37 for the ANN model compared to 0.64 for the model of Ref. [11]), rather satisfactory predictive performance has been achieved with the ANN model.

Nucl.	Exp. Data	T_{β^-} (ms)		
		ANN Model [1]	$pnQRPA+ffGT$ [11]	$DF3+CQRPA$ [12]
Nuclides around the N=50 shell closure				
^{61}Ti	15 ± 4 [29]	27.65	22.18	3.4
^{64}V	19 ± 8 [29]	23.38	7.62	3.7
^{71}Fe	28 ± 15 [29]	66	148	-
^{73}Co	41 ± 4 [29]	104	31	-
^{74}Co	19 ± 7 [29]	89	23	-
^{75}Co	30 ± 11 [28]	55	19	-
^{77}Ni	128^{+27}_{-33} [27]	79	208	144
^{78}Ni	110^{+100}_{-60} [27]	57	224	108
^{80}Cu	170^{+110}_{-50} [28]	116	85	-
Nuclides around the N=82 shell closure				
^{100}Kr	7^{+11}_{-3} [30]	16	42	-
^{103}Sr	68^{+48}_{-20} [30]	47	33	-
^{104}Sr	43^{+9}_{-7} [30]	23	71	-
^{105}Sr	40^{+36}_{-13} [30]	21	45	-
^{105}Y	83^{+5}_{-4} [30]	58	46	-
^{106}Y	62^{+25}_{-14} [30]	61	34	-
^{107}Y	41^{+15}_{-9} [30]	26	29	-
^{108}Y	25^{+66}_{-10} [30]	33	22	-
^{106}Zr	186^{+11}_{-10} [30]	106	322	-
^{107}Zr	138 ± 4 [30]	75	177	-
^{108}Zr	73 ± 4 [30]	36	162	-
^{109}Zr	63^{+38}_{-17} [30]	32	108	-
^{110}Zr	37^{+17}_{-9} [30]	16	76	-
^{111}Nb	51^{+6}_{-5} [30]	42	151	-
^{112}Nb	33^{+9}_{-6} [30]	51	75	-
^{111}Mo	200^{+40}_{-35} [32]	145	808	146
^{112}Mo	120^{+13}_{-11} [30]	71	581	-
^{113}Mo	78^{+6}_{-5} [30]	58	121	-
^{114}Mo	60^{+13}_{-9} [30]	29	103	-
^{115}Mo	51^{+79}_{-19} [30]	27	49	-
$^{115}\text{Tc}^*$	83^{+20}_{-13} [30]	84	71	134
^{116}Tc	56^{+15}_{-10} [30]	95	44	-

^{117}Tc	89^{+95}_{-30} [30]	37	40	-
^{116}Ru	204^{+32}_{-29} [31]	188	540	193
^{117}Ru	142^{+18}_{-17} [31]	129	163	127
$^{118}\text{Ru}^*$	123^{+48}_{-35} [31]	69	212	95
^{119}Rh	171 ± 18 [31]	209	108	146
$^{120}\text{Rh}^*$	136^{+14}_{-13} [31]	196	83	-
$^{121}\text{Rh}^*$	151^{+67}_{-58} [31]	91	62	87
^{121}Pd	285 ± 24 [31]	334	1275	262
$^{122}\text{Pd}^*$	175 ± 16 [31]	227	951	184
^{123}Pd	174^{+38}_{-34} [31]	149	397	143
$^{124}\text{Pd}^*$	38^{+38}_{-19} [31]	124	289	105
^{133}Cd	57 ± 10 [42]	57	185	47
^{138}Sn	150 ± 60 [38]	113	336	240
^{138}Sb	350 ± 15 [37]	144	597	-
^{139}Sb	93^{+14}_{-3} [37]	146	502	-
Nuclides around the N=126 shell closure				
^{194}Re	$1^{+0.5}_{-0.5}$ (s) [26]	20.8 (s)	70.8 (s)	2.1 (s)
^{195}Re	6^{+1}_{-1} (s) [26]	23.9 (s)	3.3 (s)	8.5 (s)
^{196}Re	3^{+1}_{-2} (s) [26]	8.8 (s)	3.6 (s)	1.4 (s)
^{199}Os	5^{+4}_{-2} (s) [26]	13.6 (s)	106.8 (s)	6.6 (s)
^{200}Os	6^{+4}_{-3} (s) [26]	21.7 (s)	187.1 (s)	6.9 (s)
^{199}Ir	6^{+5}_{-4} (s) [26]	73 (s)	370.6 (s)	46.7 (s)
^{200}Ir	43^{+6}_{-5} (s) [26]	18.2 (s)	124.1 (s)	25.0 (s)
^{201}Ir	21 ± 5 (s) [26]	20.5 (s)	130.0 (s)	28.4 (s)
^{202}Ir	11^{+3}_{-3} (s) [26]	8.6 (s)	68.4 (s)	9.8 (s)
^{203}Pt	22 ± 4 (s) [26]	32.8 (s)	654.0 (s)	12.7 (s)
^{204}Pt	16^{+6}_{-5} (s) [26]	76.2 (s)	321.8 (s)	7.4 (s)
σ_{rms}		0.37	0.64	-

TABLE II: Beta-decay half-lives T_{β^-} of recently measured r-process nuclides beyond NUBASE03 [8] as produced by the ANN model, in comparison with experimental values and with results from available $pn\text{QRPA}+ff\text{GT}$ [11] and $\text{DF3}+\text{CQRPA}$ [12] calculations. The overall error measures σ_{rms} for ANN and $pn\text{QRPA}+ff\text{GT}$ models are given in the table. Results marked with stars are also given in Table IX of Ref. [1].

In Table III we present the ANN predictions along with calculated $pn\text{QRPA}+ff\text{GT}$ [11] values for the β^- half-lives of nuclides newly identified by the PRESPEC collaboration at the GSI FRS/ESR facility. First we list the half-life values forecast by the two models for nuclides in the $N = 82$ region (namely $^{122-125}\text{Rh}$, $^{125-128}\text{Pd}$) that are under study in experiment S323 [23, 41] (under analysis). These predictions are also plotted in Figs. 7 and 8, respectively. The waiting-point nucleus ^{128}Pd acts as a bottleneck of the r-process and its decay has implications for the predictions of the Th and U cosmochronometers. It should be mentioned that $^{123-124}\text{Rh}$ and $^{127-128}\text{Pd}$ have also been identified at RIKEN [25]. Second, we list the predicted T_{β^-} values of 14 newly identified nuclides in the $N = 126$ region (namely $^{205-206}\text{Ir}$, $^{208-209}\text{Pt}$, $^{208-211}\text{Au}$, $^{213-214}\text{Hg}$, $^{213-216}\text{Tl}$) that have been included in experiment S410 [24, 41] (under analysis).

In Table IV we present the β^- half-life predictions of the ANN and $pn\text{QRPA}+ff\text{GT}$ [11] models for heavy neutron-rich newly produced at RIKEN and GSI, whose half-lives have not yet been measured. First, we list the statistical/theoretical forecasts for the 41 out of 45 nuclides that are being studied at RIKEN's RIBF by means of in-flight fission of a ^{238}U beam (from NP0702-

RIBF20) [25]. (Beta half-lives of the remaining four nuclides have already been measured; their values can be found in Table II). Most of these nuclides are considered to play a role in the r-process. Second, we list the predictions of the two models for the half-lives of 55 out of 75 heavy neutron-rich nuclides approaching the $A \simeq 195$ region (between Yb and Fr) that have been identified at GSI by the RISING collaboration using cold-fragmentation reactions of ^{238}U and ^{208}Pb projectiles of relativistic energies and the fragment separator spectrometer FRS [26, 40]. Of the remaining 20 nuclides, 11 already have measured half-lives and 9 are included in the S410 experiment; for these we have entered half-life predictions of both models in Table II and Table III, respectively. Comparing the predictions of the two models, it is found that in most cases the $pn\text{QRPA}+ff\text{GT}$ [11] model gives longer half-lives than the ANN model.

IV. CONCLUSIONS

The study of r-process nucleosynthesis is currently among the most vibrant areas of research in nuclear astrophysics. It is also one of the most challenging, as

TABLE III. Beta-decay half-lives T_{β^-} of nuclides relevant for the r-process that are under study at GSI (experiments S323 [23] and S410 [24]), as predicted by the ANN and $pnQRPA+ffGT$ [11] models.

Nucleus	$T_{\beta^-} (ms)$	
	ANN Model [1]	$pnQRPA+ffGT$ [11]
	Ref. [23]	
^{122}Rh	99.7	53.5
^{123}Rh	54.9	47.9
^{124}Rh	67.4	31.0
^{125}Rh	46.4	25.3
^{125}Pd	99.4	265.4
^{126}Pd	92.5	221.7
^{127}Pd	76.6	210.1
^{128}Pd	81.1	74.2
	Ref. [24]	
^{205}Ir	5.1 (s)	6.1(s)
^{206}Ir	3.4 (s)	2.9 (s)
^{208}Pt	8.8 (s)	7.1 (s)
^{209}Pt	4.2 (s)	3.7 (s)
^{208}Au	8.7 (s)	8.5 (s)
^{209}Au	9.0 (s)	7.50 (s)
^{210}Au	5.4 (s)	313.6
^{211}Au	5.4 (s)	2.3 (s)
^{213}Hg	7.0 (s)	4.7 (s)
^{214}Hg	9.5 (s)	3.1 (s)
^{213}Tl	18.2 (s)	32.4(s)
^{214}Tl	9.1 (s)	14.4 (s)
^{215}Tl	9.4 (s)	7.8 (s)
^{216}Tl	5.8 (s)	2.8 (s)

key issues remain open with respect to both the nature of the astrophysical setting and the nuclear physics input, which entails knowledge of nuclear behavior far from the valley of stability. This paper has been concerned with the latter aspect of r-process physics, as manifested in the β^- -decay half-lives of nuclei that are believed to play important roles in the r-process under different astrophysical scenarios. We have explored, in quantitative detail, the predictive capacity of a statistical global model of β^- -decay systematics referred to as the standard ANN model [1]. This model is an artificial neural network (ANN) of feedforward multilayer perceptron architecture that has been trained to map a given nuclidic input (Z, N) to an output encoding the corresponding β^- half-life T_{β^-} of the nuclear ground state. The training is performed by advanced algorithms for supervised learning based on a subset of data selected at random from NUBASE03, which tabulates β^- half-lives measured before November 2003. Good quality of the ANN model is substantiated in its values for the performance measure provided by the root-mean-square error σ_{rms} , namely 0.53, 0.60, and 0.65 on the training, validation, and test sets of data selected from NUBASE03.

Predictive power (“extrapability”) is properly measured by performance on test nuclei *outside* the training

and validation sets, since such nuclides have no influence on the development of the statistical model. Of special interest in the present context is the predictive performance on r-process nuclides studied at rare-isotope-beam facilities since the publication of NUBASE03. It should be emphasized that the half-lives produced by the standard ANN model that appear in Tables II-IV are all *true predictions* in this sense, because they only involve target nuclides *beyond* NUBASE03.

In addition to comparing the half-lives produced by the data-driven ANN model with available experimental β^- half-lives, it is of obvious importance to compare both the behavior of its outputs and the quality of its performance with that of established theory-thick nuclear models. With respect to behavior, the general trend of such a comparison is exemplified in the finding that the half-life values given by the standard ANN model are lower than those obtained in the $pnQRPA+ffGT$ calculations of Möller et al. [11] and closer to those from the DF3+CQRPA [12] calculations. The odd-even staggering effect is less pronounced than that found in Ref. [11]. The relative values of the root-mean-square error σ_{rms} characterizing the ANN and $pnQRPA+ffGT$ half-life predictions for the set of all nuclides with half-lives measured subsequent to NUBASE03 (cf. Table II), respectively 0.37 and 0.64, are symptomatic of good extrapolability for the ANN model. A number of additional tests of the reliability of the standard ANN model have been reported in Ref. [1].

In conclusion, the available evidence indicates that the theory-thin ANN statistical global model of β^- half-lives explored in the present work can provide a robust tool for generating nuclear input to r-process clock and matter-flow studies, and therefore serves to *complement* conventional theory-thick nuclear modeling. Naturally, the traditional models will continue to be superior in revealing the underlying physics responsible for the values taken by the targeted nuclear observables.

A promising strategy for further improvement of statistical global modeling of β^- -decay systematics lies in the development of a hybrid ANN model that targets the set of *differences* between true or experimental half-life values and the corresponding values generated by a conventional theory-thick model (e.g., that of Möller et al. [11]). Such an approach has had demonstrable success in global modeling of atomic masses [43]. Advances in predictive accuracy may also be sought through committee-machine strategies, in which different ANNs are built to process given input patterns and decide on the best output by a voting process.

V. ACKNOWLEDGMENTS

This research has been supported in part by the University of Athens under Grant No. 70/4/3309. The authors wish to thank I. N. Borzov, T. Marketin, P. Möller, and P. Ring for supplying us with theoretical data and

for helpful discussions and/or correspondence.

-
- [1] N. J. Costiris, E. Mavrommatis, K. A. Gernoth, and J. W. Clark, *Phys. Rev.* **C80**, 044332 (2009).
- [2] E. M. Burbidge, G. R. Burbidge, W. A. Fowler, and F. Hoyle, *Rev. Mod. Phys.* **29**, 547 (1957); ; A. G. W. Cameron, *ApJ* 62, 138 (1957).
- [3] F. Kappeler, F. K. Thielemann, and M. Wiescher, *Ann. Rev. Nucl. Part. Sci.* **48**, 175 (1998).
- [4] M. Arnould, S. Goriely, and K. Takahashi, *Phys. Rep.* **450**, 97 (2007).
- [5] K.-L. Kratz, K. Farouqi, and B. Pfeiffer, *Progr. Part. Nucl. Phys.* **59**, 147 (2007).
- [6] F.-K. Thielemann, A. Arcones, R. Kppeli, M. Liebendrerfer, T. Rauscher, C. Winteler, C. Frhlich, I. Dillmann, T. Fischer, G. Martinez-Pinedo, K. Langanke, K. Farouqi, K.-L. Kratz, I. Panov, and I. Korneev, *Progr. Part. Nucl. Phys.* **66**, 346 (2011).
- [7] Y.-Z. Qian, (2012), [arXiv:1201.5112 \[astro-ph.SR\]](https://arxiv.org/abs/1201.5112).
- [8] G. Audi, O. Bersillon, J. Blachot, and A. Wapstra, *Nucl. Phys.* **A729**, 3 (2003).
- [9] RIBF web page <http://www.nishina.riken.jp/RIBF/>, FAIR web page <http://www.fair-center.eu>, FRIB web page <http://www.frib.msu.edu>.
- [10] J. J. Cuenca-Garcia, G. Martinez-Pinedo, K. Langanke, F. Nowacki, and I. N. Borzov, *Eur. Phys. J.* **A34**, 99 (2007).
- [11] P. Möller, B. Pfeiffer, and K.-L. Kratz, *Phys. Rev.* **C67**, 055802 (2003), <http://t2.lanl.gov/molleretal/publications/tpnff.dat>
- [12] P. Möller, private communication 2011.
- [13] I. N. Borzov, *Phys. Rev.* **C67**, 025802 (2003), private communication 2010, 2011.
- [14] I. N. Borzov, J. J. Cuenca-Garcia, K. Langanke, G. Martinez-Pinedo, and F. Montes, *Nucl. Phys.* **A814**, 159 (2008).
- [15] T. Marketin, D. Vretenar, and P. Ring, *Phys. Rev.* **C75**, 024304 (2007); ; T. Marketin and P. Ring, private communication 2011.
- [16] J. W. Clark, in *Scientific Applications of Neural Nets*, edited by J. W. Clark, T. Lindenau, and M. L. Ristig (Springer-Verlag, Berlin, 1999) p. 1.
- [17] K. A. Gernoth, in *Scientific Applications of Neural Nets*, edited by J. W. Clark, T. Lindenau, and M. L. Ristig (Springer-Verlag, Berlin, 1999) p. 139.
- [18] E. Mavrommatis, A. Dakos, K. A. Gernoth, and J. W. Clark, in *Condensed Matter Theories*, Vol. 13, edited by J. da Providencia and F. B. Malik, Commack (Nova Science Publishers, New York, 1998) pp. 423–438.
- [19] J. W. Clark, E. Mavrommatis, S. Athanasopoulos, A. Dakos, and K. Gernoth, (2001), [arXiv:nucl-th/0109081 \[nucl-th\]](https://arxiv.org/abs/nucl-th/0109081).
- [20] S. Haykin, *Neural Networks: A Comprehensive Foundation* (McMillan, N.Y., 1993).
- [21] C. M. Bishop, *Neural Networks for Pattern Recognition* (Clarendon, Oxford, 1995).
- [22] D. Nguyen and B. Widrow, in *Proc. of the Int. Joint Conf. on Neural Networks*, Vol. 3 (1990) pp. 21–26.
- [23] H. Klapdor, *Progr. Part. Nucl. Phys.* **10**, 131 (1983).
- [24] F. Montes and et al., GSI experiment proposal **S323**.
- [25] J. Tain and et al., GSI experiment proposal **S410**.
- [26] T. Ohnishi, T. Kubo, K. Kusaka, A. Yoshida, K. Yoshida, M. Ohtake, N. Fukuda, H. Takeda, D. Kameda, K. Tanaka, N. Inabe, Y. Yanagisawa, Y. Gono, H. Watanabe, H. Otsu, H. Baba, T. Ichihara, Y. Yamaguchi, M. Takechi, S. Nishimura, H. Ueno, A. Yoshimi, H. Sakurai, T. Motobayashi, T. Nakao, Y. Mizoi, M. Matsushita, K. Ieki, N. Kobayashi, K. Tanaka, Y. Kawada, N. Tanaka, S. Deguchi, Y. Satou, Y. Kondo, T. Nakamura, K. Yoshinaga, C. Ishii, H. Yoshii, Y. Miyashita, N. Uematsu, Y. Shiraki, T. Sumikama, J. Chiba, E. Ideguchi, A. Saito, T. Yamaguchi, I. Hachiuma, T. Suzuki, T. Moriguchi, A. Ozawa, T. Ohtsubo, M. A. Famiano, H. Geissel, A. S. Nettleton, O. B. Tarasov, D. P. Bazin, B. M. Sherrill, S. L. Manikonda, and J. A. Nolen, *J. Phys. Soc. Jap.* **79**, 073201 (2010).
- [27] J. Benlliure, H. Alvarez, T. Kurtukian, A. Morales, K. Schmidt, *et al.*, in *PoS(NIC XI)084* (Heidelberg, Germany, 2010); ; J. Benlliure, A. Morales, T. Kurtukian-Nieto, *et al.*, in EFN 2010 (San Lorenzo del Escorial, Spain, 2010) RISING Collaboration.
- [28] P. T. Hosmer, H. Schatz, A. Aprahamian, O. Arndt, R. R. C. Clement, A. Estrade, K.-L. Kratz, S. N. Liddick, P. F. Mantica, W. F. Mueller, F. Montes, A. C. Morton, M. Ouellette, E. Pellegrini, B. Pfeiffer, P. Reeder, P. Santi, M. Steiner, A. Stolz, B. E. Tomlin, W. B. Walters, and A. Wöhr, *Phys. Rev. Lett.* **94**, 112501 (2005).
- [29] P. Hosmer, H. Schatz, A. Aprahamian, O. Arndt, R. R. C. Clement, A. Estrade, K. Farouqi, K.-L. Kratz, S. N. Liddick, A. F. Lisetskiy, P. F. Mantica, P. Möller, W. F. Mueller, F. Montes, A. C. Morton, M. Ouellette, E. Pellegrini, J. Pereira, B. Pfeiffer, P. Reeder, P. Santi, M. Steiner, A. Stolz, B. E. Tomlin, W. B. Walters, and A. Wöhr, *Phys. Rev.* **C82**, 025806 (2010).
- [30] J. M. Daugas, I. Matea, J.-P. Delaroche, M. Pfützner, M. Sawicka, F. Becker, G. Bélier, C. R. Bingham, R. Borcea, E. Bouchez, A. Buta, E. Dragulescu, G. Georgiev, J. Giovinazzo, M. Girod, H. Grawe, R. Grzywacz, F. Hammache, F. Ibrahim, M. Lewitowicz, J. Libert, P. Mayet, V. Méot, F. Negoita, F. de Oliveira Santos, O. Perru, O. Roig, K. Rykaczewski, M. G. Saint-Laurent, J. E. Sauvestre, O. Sorlin, M. Stanoiu, I. Stefan, C. Stodel, C. Theisen, D. Verney, and J. Żylicz, *Phys. Rev. C* **83**, 054312 (2011).
- [31] S. Nishimura, Z. Li, H. Watanabe, K. Yoshinaga, T. Sumikama, T. Tachibana, K. Yamaguchi, M. Kurata-Nishimura, G. Lorusso, Y. Miyashita, A. Odahara, H. Baba, J. S. Berryman, N. Blasi, A. Bracco, F. Camera, J. Chiba, P. Doornenbal, S. Go, T. Hashimoto, S. Hayakawa, C. Hinke, E. Ideguchi, T. Isobe, Y. Ito, D. G. Jenkins, Y. Kawada, N. Kobayashi, Y. Kondo, R. Krücken, S. Kubono, T. Nakano, H. J. Ong, S. Ota, Z. Podolyák, H. Sakurai, H. Scheit, K. Steiger, D. Steppenbeck, K. Sugimoto, S. Takano, A. Takashima, K. Tajiri, T. Teranishi, Y. Wakabayashi, P. M. Walker, O. Wieland, and H. Yamaguchi, *Phys. Rev. Lett.* **106**, 052502 (2011).

- [31] F. Montes, A. Estrade, P. T. Hosmer, S. N. Liddick, P. F. Mantica, *et al.*, **Phys. Rev. C** **73**, 035801 (2006).
- [32] J. Pereira, S. Hennrich, A. Aprahamian, O. Arndt, A. Becerril, T. Elliot, A. Estrade, D. Galaviz, R. Kessler, K.-L. Kratz, G. Lorusso, P. F. Mantica, M. Matos, P. Möller, F. Montes, B. Pfeiffer, H. Schatz, F. Schertz, L. Schnorrenberger, E. Smith, A. Stolz, M. Quinn, W. B. Walters, and A. Wöhr, **Phys. Rev. C** **79**, 035806 (2009).
- [33] B. Pfeiffer, K.-L. Kratz, F.-K. Thielemann, and W. B. Walters, **Nuc. Phys. A** **693**, 282 (2001).
- [34] M. Terasawa, K. Langanke, T. Kajino, G. J. Mathews, and E. Kolbe, **ApJ** **608**, 470 (2004), ; J. J. Cowan, F.-K. Thielemann, and J. W. Truran, *Phys. Rep.* **208**, 267 (1991).
- [35] C. Sneden, J. J. Cowan, J. E. Lawler, I. I. Ivans, S. Burles, T. C. Beers, F. Primas, V. Hill, J. W. Truran, G. M. Fuller, B. Pfeiffer, and K.-L. Kratz, **ApJ** **591**, 936 (2003).
- [36] C. Travaglio, R. Gallino, E. Arnone, J. Cowan, F. Jordan, and C. Sneden, **ApJ** **601**, 864 (2004).
- [37] O. Arndt, K.-L. Kratz, W. B. Walters, K. Farouqi, U. Köster, V. Fedosseev, S. Hennrich, C. J. Jost, A. Wöhr, A. A. Hecht, B. Pfeiffer, J. Shergur, and N. Hoteling, **Phys. Rev. C** **84**, 061307 (2011).
- [38] K. Kratz, B. Pfeiffer, O. Arndt, S. Hennrich, A. Wöhr, and the ISOLDE/IS333/IS378/IS393 Collaborations, **Euro. Phys. J. A** **25**, 633 (2005).
- [39] T. Kurtukian-Nieto, J. Benlliure, K.-H. Schmidt, L. Audouin, F. Becker, B. Blank, I. Borzov, E. Casarejos, M. F.-O. nez, J. Giovinazzo, D. Henzlova, B. Jurado, K. Langanke, G. Martinez-Pinedo, J. Pereira, F. Rejmund, and O. Yordanov, **Nucl. Phys. A** **827**, 587c (2009).
- [40] H. Alvarez-Pol, J. Benlliure, E. Casarejos, L. Audouin, D. Cortina-Gil, T. Enqvist, B. Fernández-Domínguez, A. R. Junghans, B. Jurado, P. Napolitani, J. Pereira, F. Rejmund, K.-H. Schmidt, and O. Yordanov, **Phys. Rev. C** **82**, 041602 (2010).
- [41] I. Dillmann and Y. A. Litvinov, **Prog. Part. Nucl. Phys.** **66**, 358 (2011).
- [42] O. Arndt, Diploma Thesis, University of Mainz (2003).
- [43] S. Athanassopoulos, E. Mavrommatis, K. Gernoth, and J. W. Clark, (2005), [arXiv:nucl-th/0511088](https://arxiv.org/abs/nucl-th/0511088) [[nucl-th](https://arxiv.org/abs/nucl-th/0511088)].

TABLE IV. Beta-decay half-lives T_{β^-} of nuclides relevant for the r-process that have recently been identified at RIKEN [25] and at GSI [26, 40], as predicted by the ANN and $pnQRPA+ffGT$ [11] models.

Nucleus	T_{β^-} (ms)		Nucleus	T_{β^-} (ms)	
	ANN Model [1] Ref. [25]	$pnQRPA+ffGT$ [11]		ANN Model [1] Ref. [26, 40]	$pnQRPA+ffGT$ [11]
⁷¹ Mn	27.1	8.1	¹⁹² Ta	4.9 (s)	0.5 (s)
⁷³ Fe	38.2	56.1	¹⁹³ Ta	5.0 (s)	1.4 (s)
⁷⁴ Fe	31.3	47.0	¹⁹³ W	15.2 (s)	12.8 (s)
⁷⁶ Co	58.5	15.4	¹⁹⁴ W	24.2 (s)	19.9 (s)
⁷⁹ Ni	39.2	37.6	¹⁹⁵ W	6.8 (s)	13.3 (s)
⁸¹ Cu	52.0	80.8	¹⁹⁷ Re	9.4 (s)	4.5 (s)
⁸² Cu	67.2	29.3	¹⁹⁸ Re	4.9 (s)	2.0 (s)
⁸⁴ Zn	35.9	154.9	¹⁹⁸ Os	94.5 (s)	601.2 (s)
⁸⁵ Zn	31.9	19.4	²⁰¹ Os	6.6 (s)	81.1 (s)
⁸⁷ Ga	38.7	68.5	²⁰³ Ir	9.0 (s)	34.9 (s)
⁹⁰ Ge	20.6	43.0	²⁰⁵ Pt	12.8 (s)	20.6 (s)
⁹⁵ Se	27.4	25.8	²⁰⁶ Au	17.0 (s)	21.3 (s)
⁹⁸ Br	44.4	29.0	²⁰⁷ Au	18.8 (s)	22.3 (s)
¹⁰¹ Kr	16.1	14.3	²¹¹ Hg	12.6 (s)	14.9
¹⁰³ Rb	18.2	16.5	²¹² Hg	21.1 (s)	10.5
¹⁰⁶ Sr	10.7	39.7	²¹⁵ Hg	4.5 (s)	0.2 (s)
¹⁰⁷ Sr	10.9	28.0	²¹⁷ Tl	5.7 (s)	1.3 (s)
¹⁰⁹ Y	12.9	18.4	²¹⁵ Pb	27.7 (s)	282.5 (s)
¹¹¹ Zr	15.8	50.7	²¹⁶ Pb	67.0 (s)	852.2 (s)
¹¹² Zr	9.1	42.7	²¹⁷ Pb	12.9 (s)	104.9 (s)
¹¹⁴ Nb	27.2	21.0	²¹⁸ Pb	22.4 (s)	66.3 (s)
¹¹⁵ Nb	11.1	15.5	²¹⁹ Pb	7.5 (s)	1.2 (s)
¹¹⁶ Mo	15.6	50.6	²²⁰ Pb	10.4 (s)	7.0 (s)
¹¹⁷ Mo	14.7	42.9	²¹⁹ Bi	18.5 (s)	26.5 (s)
¹¹⁹ Tc	20.6	25.1	²²⁰ Bi	9.6 (s)	5.2 (s)
¹²⁰ Tc	28.0	21.8	²²¹ Bi	10.0 (s)	9.7 (s)
¹²¹ Ru	31.8	88.3	²²² Bi	6.3 (s)	2.0 (s)
¹²² Ru	26.4	68.6	²²³ Bi	6.2 (s)	3.5 (s)
¹²³ Ru	24.5	50.6	²²⁴ Bi	4.5 (s)	2.4 (s)
¹²⁴ Ru	24.1	45.0	²²¹ Po	27.8 (s)	3.2 (s)
¹²³ Rh	54.9	47.9	²²² Po	70.9 (s)	27.3 (s)
¹²⁴ Rh	67.4	31.0	²²³ Po	13.7 (s)	4.4 (s)
¹²⁵ Rh	46.4	25.3	²²⁴ Po	24.9 (s)	11.1 (s)
¹²⁶ Rh	57.7	26.0	²²⁵ Po	8.1 (s)	5.7 (s)
¹²⁷ Pd	76.6	210.1	²²⁶ Po	11.8 (s)	3.0 (s)
¹²⁸ Pd	81.1	74.2	²²⁷ Po	5.4 (s)	2.4 (s)
¹⁴⁰ Sb	82.0	359.1	²²⁴ At	17.7 (s)	4.1 (s)
¹⁴³ Te	112.3	63.8	²²⁵ At	19.5 (s)	5.1 (s)
¹⁴⁵ I	147.8	55.2	²²⁶ At	10.4 (s)	3.3 (s)
¹⁴⁸ Xe	159.6	116.8	²²⁷ At	10.8 (s)	8.1 (s)
¹⁵² Ba	261.2	191.2	²²⁸ At	6.9 (s)	2.1 (s)
	Ref. [26, 40]		²²⁹ At	6.9 (s)	1.7 (s)
¹⁸³ Yb	7.9 (s)	31.8 (s)	²³⁰ At	4.9 (s)	0.7 (s)
¹⁸⁴ Yb	9.4 (s)	24.9 (s)	²²⁹ Rn	14.8 (s)	21.8 (s)
¹⁸⁶ Lu	5.0 (s)	2.1 (s)	²³⁰ Rn	28.7 (s)	12.6 (s)
¹⁸⁷ Lu	5.2 (s)	1.4 (s)	²³¹ Rn	8.9 (s)	3.9 (s)
¹⁸⁹ Hf	7.2 (s)	1.2 (s)	²³² Rn	13.7 (s)	4.5 (s)
¹⁹⁰ Hf	8.8 (s)	4.0 (s)	²³³ Fr	11.9 (s)	9.4 (s)
¹⁹¹ Ta	10.2 (s)	1.6 (s)			